

Size effect and strain rate sensitivity in benzocyclobutene film

D.-L. Liu, T.-M. Lu, and G.-C. Wang

Department of Physics, Applied Physics and Astronomy, Rensselaer Polytechnic Institute, Troy, New York 12180-3590

R. C. Picu^{a)}

Department of Mechanical, Aerospace and Nuclear Engineering, Rensselaer Polytechnic Institute, Troy, New York 12180-3590

(Received 13 May 2004; accepted 19 August 2004)

The mechanical properties of benzocyclobutene film are investigated at the nanoscale by nano-indentation using atomic force microscopy (AFM). The force versus indentation depth data were collected with two different AFM tips of radii ~ 20 and ~ 380 nm. A strong size effect of the plastic flow stress was observed as the radius of the indenter tip was reduced. More important, the material exhibited pronounced strain rate sensitivity when probed at the nanoscale, while it was rate insensitive at larger scales. These two size effects were quantified by analytic and finite element modeling. © 2004 American Institute of Physics. [DOI: 10.1063/1.1805710]

The constitutive behavior of most materials becomes size dependent when the dimension of the specimen or the probed volume becomes of the order of a few microns. The smaller samples were stronger (higher yield stress) than the larger ones.¹ The size effect of the yield stress was observed as early as 1994 in a set of careful experiments performed on thin metallic wires.² Size effects were also observed in strain hardening (flow stress) and in the ultimate tensile strength.³ Small volumes of material exhibit higher strain hardening rates and fail at larger stresses. These phenomena are observed in nano-indentation tests as well as when an internal length scale of the material is controlled. An example from this last category is that of nanostructured materials in which the grain size is reduced into the tens of nanometers range.⁴

Nanoindentation testing is a popular technique widely used for the estimation of mechanical properties of materials at the nanoscale. The test is a replica of the traditional indentation test in which the load versus displacement and the load versus contact area are used to determine the hardness of the material.⁵ One of the limitations of nano-indentation is that no high resolution imaging of the area to be probed is possible before or after the test, since the tip radius is rather large (micron size). Therefore it is difficult to use the nanoindenter to relate the indentation test results to details of the surface structure. An alternative is provided by the use of the atomic force microscope (AFM) for both the surface imaging and depth sensing. The AFM can accurately monitor loads in the nano-Newton range while concomitantly monitoring the indentation depth. The image resolution and sensing accuracy of the force and displacement by an AFM make it a powerful technique for studying the local interaction of the tip with the surface. This technique was recently used to test the mechanical behavior of isolated free-standing nano-structures⁶ and thin film coatings.⁷⁻⁹

In this letter, the mechanical properties of benzocyclobutene (BCB) polymer film are investigated by AFM indentation. Two size effects are evidenced: one controlling the plastic deformation, the other controlling the strain rate sensitivity of the material. Modeling of the indentation process is performed to separate and quantify the two size effects.

BCB, also known as divinylsiloxane bis(benzocyclobutene), is a thermoset resin derivative of cyclobutane. When heated, the four-member ring of the BCB monomer opens to produce a very reactive intermediate diene, which undergoes Diels-Alder reactions with available dienophiles (C=C). The multiple reactive sites (two C=C and two cyclobutane rings) on BCB monomer lead to the formation of a highly cross-linked three-dimensional network with an isotropic dielectric constant of 2.65. The low dielectric constant of BCB makes it highly desirable for microelectronics applications such as the dielectric isolation of Cu and Al multilayer interconnects deposited on Si, ceramic, or laminate substrates.

The manufacturer, Dow Chemical, reports results from mechanical testing of free-standing BCB films of thickness larger than 0.5 mm.¹⁰ The Young's modulus and the Poisson's ratio measured at room temperature were approximately 2.9 and 0.34 GPa, respectively. The thick film exhibited plastic deformation up to an engineering failure strain of 8%, a yield stress (measured in uniaxial tension) of ~ 40 MPa, and pronounced strain hardening. The failure stress was 95 MPa. Most important for the present discussion, the material exhibited *no measurable strain rate sensitivity* and no viscoelastic recovery upon loading up to and unloading from stresses smaller than the failure stress. The glass transition temperature was larger than 350°C.

The BCB film was prepared by a spin-on deposition technique. BCB was originally prepared as a solution and was dispensed onto the Si wafer surface in predetermined amounts. The wafer was subjected to rapid spinning with a spin speed of 3500 rpm for 20–30 s. Subsequent heating at low temperature (200°C for ~ 2 h) led to solvent evaporation and promoted cross-linking. High resolution AFM imaging (500 nm \times 500 nm) of the film indicated that the surface rms roughness is ~ 0.28 nm. The film thickness measured by an ellipsometry was ~ 1200 nm.

The nano-indentation experiment was performed with an atomic force microscope (AutoProbe CP, Park Scientific Instruments, TM Microscope). Triangular as well as rectangular silicon cantilevers with silicon conical tips were used in the experiment. The spring constants k were calibrated before the test and the values were 17 and 34 N/m.¹¹ During an indentation, the applied force F is given by $F=ky$, where

^{a)} Author to whom correspondence should be addressed; electronic mail: picu@rpi.edu

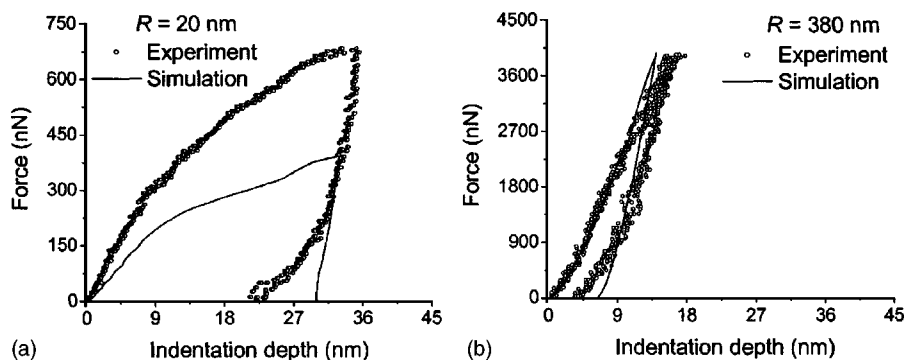


FIG. 1. Typical force vs indentation depth curves for a BCB film. (a) Tip radius $R=20$ nm. (b) $R=380$ nm. The experimental data points are solid dots and the finite element modeling results are solid curves. The model uses the constitutive law measured at the macroscopic scale.

y is the cantilever deflection, while the indentation depth d is obtained from the relationship $d=z-y$, with z being the extension of the piezoelectric scanner tube. Hence, the instrument measures independently both the indentation force and the penetration depth. In order to correlate the force with the indentation depth correctly, calibration was performed every time prior to the measurement. This cantilever calibration procedure requires taking a force versus distance measurement using a hard sapphire substrate in which the tip does not penetrate ($d=0$). At first, a $2\ \mu\text{m} \times 2\ \mu\text{m}$ AFM image was taken. Then the rastering of the scanner was stopped, the AFM was turned to contact mode, and the indentation was performed. Due to the variability in material properties, the force versus indentation depth curves taken at different locations differ and averaging is required. In our experiment, clean samples were used in ambient for which the thickness of the water layer was estimated to be ~ 0.2 nm.¹² The 0.2 nm is much smaller than the indentation depth and its effect on the force versus depth may be ignored. The radius of curvature R of the tip was characterized by imaging a tip characterizer.¹³ The tip radius is 20 nm with a semiapical angle of 12° for the 17 N/m cantilever and the tip radius is 380 nm with a semiapical angle of 17° for the 34 N/m cantilever. The tip was characterized before and after an indentation. The indentation rate was set from 5 to 500 nm/s in separate experiments for both types of cantilevers. In order to minimize the measurement noise due to the tip damage, each indentation was performed with a different tip.

The results of the tests are presented next. Typical force versus indentation depth curves are shown in Figs. 1(a) and 1(b) and for two indenter radii, 20 and 380 nm, respectively. The indentation velocity in these tests was 500 nm/s during both loading and unloading. Qualitative differences are observed in these two cases. The indentation with the sharp tip leads to a pronounced plastic deformation during the loading. The maximum force is on the order of 700 nN. Indentation with the blunter tip leads to very little plastic deformation

although the maximum force is about $4\ \mu\text{N}$. Due to the high indentation velocity, we conjecture that the effect of time-dependent processes in controlling these two curves is minimal. Hence, the elastic-plastic rate-independent response of the material is measured in these tests.

To gain insight into the result, the indentation was modeled using two-dimensional axisymmetric finite elements. The conical tip was modeled with exactly the same geometry as used in the experiment: semiapical angle 12° and $R=20$ nm for the 17 N/m tip; semiapical angle 17° and $R=380$ nm for the 34 N/m tip. A spring was attached to the tip and the speed/displacement of its top end was controlled to mimic the experimental conditions, i.e., the z movement of the scanner. The spring represents the cantilever and its stiffness was set accordingly. The mesh was refined until the mesh sensitivity was eliminated.

The material constitutive behavior in these simulations was defined based on results from the macroscopic tensile tests of free standing (thick) films described earlier.¹⁰ The simulated force-indentation depth curves for the two cases are shown as continuous curves in Fig. 1. The indentation curve obtained with the blunt indenter is predicted closely using the material properties measured at the large scale. However, the simulated indentation curve obtained with the sharp indenter is far from the experimental result. As expected, size effects of both yield stress and hardening behavior are observed. The material appears to be stronger when tested at the small scale.

The effect of the indentation rate on the force-indentation depth curves was studied next. Figure 2 shows typical curves obtained at indentation velocities ranging from 5 to 500 nm/s (for both loading and unloading). Interestingly, a pronounced rate effect is observed in both cases. As the rate decreases, the curves appear to shift toward larger total displacements. We note that the slight shift of the maximum of each set of curves to higher displacements and to

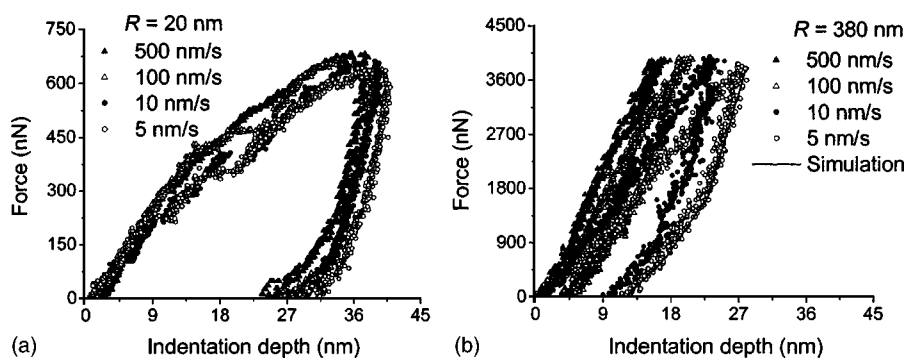


FIG. 2. Measured force vs indentation depth data for a BCB film collected under various indentation rates ranging from 5 to 500 nm/s. (a) Tip radius $R=20$ nm. (b) $R=380$ nm. The solid curve is the fit using a standard linear viscoelastic model for the unloading portion of the experimental curve for an indentation rate of 5 nm/s.

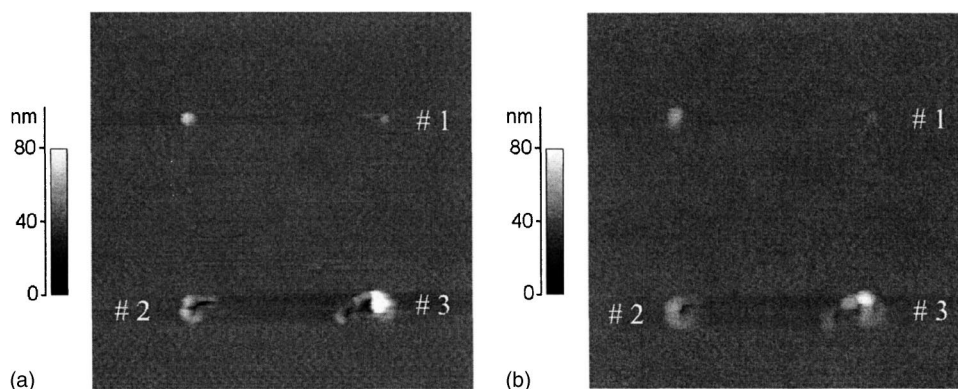


FIG. 3. AFM images of the healing of indents in a BCB film. The size of each image is $2\ \mu\text{m} \times 2\ \mu\text{m}$. (a) Image taken right after indentations. The forces applied on locations 1, 2, and 3 are 270, 450, and 800 nN, respectively. (b) Image taken 45 h after indentations.

lower loads is characteristic for a test that is neither exactly load nor displacement controlled.

This observation is in contrast with that made at larger scales according to which the material response is rate insensitive.¹⁰ This defines another size effect: when a material is probed at the nanoscale, the rate sensitivity of this material increases. Reports that underline a similar effect on rate sensitivity are by Schweiger *et al.*¹⁴ and Torre *et al.*¹⁵ Schweiger *et al.*¹⁴ observed that the rate sensitivity in nano-crystalline Ni is significantly larger than that in micro-crystalline and ultrafine crystalline Ni. They attribute the effect to the larger volume fraction of grain boundary-affected material in the nano-crystalline sample. The physical origin of the enhanced rate sensitivity in our samples is unclear at present, but since BCB is amorphous, it must be fundamentally different than that leading to the effect seen in Ni. We note that the 0.2-nm-thick water layer present on the surface of the specimen should not lead to the observed strain rate sensitivity due to its much smaller viscosity compared to that of the sample (liquid versus solid).

To quantify the rate dependence, we focus on the unloading part of the curves. The unloading is considered to be viscoelastic in nature. Specifically, we focus on the curves in Fig. 2(b) ($R=380\ \text{nm}$) for which the size effect on the plastic component of the deformation is limited. The unloading portion of the experimental curve for 5 nm/s indentation rate is fitted with the solution for indentation with a rigid spherical punch of radius R into a viscoelastic body characterized by a standard linear model (a spring in series with a Kelvin unit).¹⁶ The fit matches the experimental data well and is shown as the solid line in Fig. 2(b). The force (F) versus indentation depth (d) is given by

$$\frac{F(t)}{4\sqrt{RE}} = \frac{d^{3/2}}{a+1} \left[\int_0^{t_1/t} (1+a \exp(-(1-\xi)t/\tau)) \xi^{1/2} d\xi - \int_{t_1/t}^1 (1+a \exp(-(1-\xi)t/\tau)) (2t_1/t - \xi)^{1/2} d\xi \right],$$

where $E=2.9\ \text{GPa}$ is the macroscopically measured Young's modulus, t_1 is the time at which unloading begins, and a and τ are material parameters. The fitting returns the relaxation time constant τ to be 0.2 s and the nondimensional internal parameter $a=7$. The time constant of the macroscopic material is virtually infinite, as no rate sensitivity was observed at that scale.

Further support for the observation of finite rate sensitivity is provided by the images in Fig. 3 in which healing of indents is seen. Three indents were made with the 17 N/m

cantilever and the tip radius of 20 nm. The image size is $2\ \mu\text{m} \times 2\ \mu\text{m}$. The forces applied were 270, 450, and 800 nN on locations 1, 2, and 3, respectively. The image in Fig. 3(a) was taken right after the indents were made, while that in Fig. 3(b) was taken 45 h later. Line scans across the indents were performed and the indent depths measured immediately after the test were ~ 10 , ~ 16 , and $\sim 29\ \text{nm}$, respectively. After 45 h, the respective depths decreased to ~ 4 , ~ 10 , and $\sim 8\ \text{nm}$ showing clearly that viscoelastic recovery took place.

In conclusion, results of AFM indentation tests with both a sharp tip ($R=20\ \text{nm}$) and a blunt tip ($R=380\ \text{nm}$) of a BCB film are reported. The material was found to exhibit size effects of the yield stress and strain hardening. Furthermore, the material exhibited pronounced rate sensitivity, as observed in tests performed with indentation rates between 5 and 500 nm/s. At the macroscopic scale the material exhibits no measurable rate sensitivity. This demonstrates an unexpected size effect on rate sensitivity in addition to the expected size effect on the yield stress and strain hardening.

The authors thank Professor Ron Gutmann and Dr. Anurag Jindal for providing us the BCB samples. The work was supported by the NSF through Grant No. CMS-0324492.

¹R. Saha, Z. Xue, Y. Huang, and W. D. Nix, *J. Mech. Phys. Solids* **49**, 1997 (2001).

²N. A. Fleck, G. M. Muller, M. F. Ashby, and J. W. Hutchinson, *Acta Metall. Mater.* **42**, 475 (1994).

³Z. P. Bazant, *Scaling of Structural Strength* (Taylor & Francis, New York, 2002).

⁴See, e.g., R. A. Masumura, P. M. Hazzledine, and C. S. Pande, *Acta Mater.* **46**, 4527 (1998).

⁵W. C. Oliver and G. M. Pharr, *J. Mater. Res.* **7**, 1564 (1992).

⁶D.-L. Liu, D.-X. Ye, F. Khan, F. Tang, B.-K. Lim, R. C. Picu, G.-C. Wang, and T.-M. Lu, *J. Nanosci. Nanotechnol.* **3**, 492 (2003).

⁷S. A. Chizhik, Z. Huang, V. V. Gorbunov, N. K. Myshkin, and V. V. Tsukruk, *Langmuir* **14**, 2606 (1998).

⁸A. Opdahl and G. Somorjai, *J. Polym. Sci., Part B: Polym. Phys.* **39**, 2263 (2001).

⁹M. R. Vanlandingham, J. S. Villarrubia, and G. F. Meyers, *Polym. Prepr. (Am. Chem. Soc. Div. Polym. Chem.)* **41**, 1412 (2000).

¹⁰J. Im, E. O. Shaffer, R. Peters, T. Rey, C. Murlick, and R. L. Sammler, *Proc. SPIE* **2920**, 168 (1996).

¹¹M. Tortonesi and M. Kirk, *Proc. SPIE* **3009**, 53 (1997).

¹²M. Luna, J. Colchero, A. Gil, J. Gomez-Herrero, and A. Baro, *Appl. Surf. Sci.* **157**, 393 (2000).

¹³V. Bykov, A. Gologanov, and V. Shevyakov, *Appl. Phys. A: Mater. Sci. Process.* **66**, 499 (1998).

¹⁴F. D. Torre, H. van Swygenhoven, and M. Victoria, *Acta Mater.* **50**, 3957 (2002).

¹⁵R. Schweiger, B. Moser, M. Dao, N. Chollacoop, and S. Suresh, *Acta Mater.* **51**, 5159 (2003).

¹⁶E. H. Lee and J. R. M. Radok, *J. Appl. Mech.* **27**, 438 (1960).